BIOCHEMISTRY
including biophysical chemistry & molecular biology

ARTICLE

pubs.acs.org/biochemistry

Functional Evaluation of Bacteriophage T4 Rad50 Signature Motif Residues

Timothy J. Herdendorf and Scott W. Nelson*

Department of Biochemistry, Biophysics, and Molecular Biology, Iowa State University, Ames, Iowa 50011, United States

Supporting Information

ABSTRACT: The repair of DNA double-strand breaks (DSBs) is essential to maintaining the integrity of the genome, and organisms have evolved a conserved mechanism to facilitate their repair. In eukaryotes, archaea, and some bacteriophage, a complex made up of Mre11 and Rad50 (MR complex), which are a nuclease and ATPase, respectively, is involved in the initial processing of DSBs. Rad50 is a member of the ATP Binding Cassette (ABC) protein superfamily, the members of which contain an important Signature motif that acts *in trans* to complete the dimeric ATP binding site. To explore the functional relevance of this motif, four of its five residues were mutated in bacteriophage T4 Rad50, and their respective ATPase and nuclease activities were evaluated. The mutations reveal the functional roles of the Signature motif in ATP binding, hydrolysis, and cooperativity. In several mutants, the degree of DNA activation of ATP hydrolysis activity is reduced, indicating that the Signature motif is involved in allosteric signal transmission between the DNA and ATP binding sites of the MR complex. ATP hydrolysis is not required for nuclease activity when the probe is near the beginning of the DNA substrate; however, when an internal probe is used, decreases in ATPase activity have substantial effects on nuclease activity, suggesting that ATP hydrolysis is involved in translocation of the complex. Unexpectedly, the ATP hydrolysis and nuclease activities are not directly correlated with each other, and each mutation appears to differentially affect the exonuclease activity of Mre11.

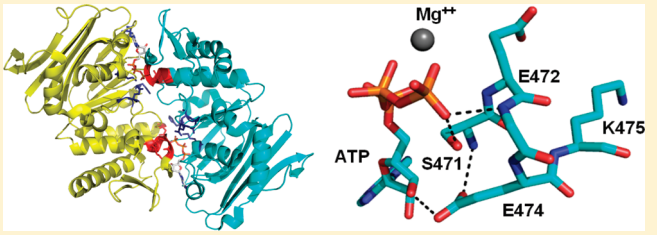

Double-strand breaks (DSBs) are among the most deleterious forms of DNA damage, and if not properly repaired they can cause chromosomal rearrangements that have the potential to induce tumorigenesis or cellular death.[1] DSBs are common and can be caused by internal and external factors. Internal DNA damaging factors can be metabolic byproducts such as reactive oxygen species or stalled protein complexes that cause collapse of the replication fork. External DNA damaging factors can be UV radiation, ionizing radiation, or a wide range of genotoxic chemicals. In addition to spontaneous DSBs that are considered a form of DNA damage, eukaryotic genomes are subject to programmed DSBs that occur during meiosis or VDJ recombination.[2]

In eukaryotes, there are three pathways for the repair of DSBs: homologous recombination (HR), nonhomologous end-joining (NHEJ), and microhomology-mediated end-joining (MMEJ).[3] NHEJ is considered to be "classic end-joining" and primarily relies on Ku70-Ku80, along with DNA ligase IV and XRCC4.[4] NHEJ can be either error-free or error-prone, the latter of which is due to small deletions or insertions at the site of DNA ligation.[5] MMEJ is Ku-independent and is always error-prone as it relies on base-pairing between microhomologies of approximately 5−25 nts that are exposed by nucleolytic trimming of the DSB.[3] HR is considered to be an error-free DSB repair pathway as it uses undamaged homologous DNA as a template for repair of the damaged DNA.[6] The homologous DNA can be a sister chromatid, a homologue (if the organism is mulitploidy), or a homologous sequence on the same or different chromosome. The Mre11/Rad50 (MR) complex is directly involved in all three of these pathways but it is best known for its role in HR, and this is the function that has been most well conserved.[7] HR is a multistep pathway that involves several dozen proteins.[8] The protein components involved in HR are best defined in the *S. cerevisiae* system.[9,10] The first step of HR is the production of a 3′ssDNA overhang and is referred to as DSB resection (the 5′ strand is resected). In eukaryotes, this step occurs in two stages. In the first stage, the MR complex, along with Xrs2 and Sae2 in *S. cerevisiae*, trims 50−100 nucleotides from the 5′ end of the DSB.[11] In the second stage, either ExoI and RPA or Sgs1/Top3/RmiI, Dna2, and RPA bind to the MR-processed DSB and proceed with an extensive (>500 nts) resection of the DSB.[12,13] Following DSB resection, Rad51, with the help of Rad52, forms a filament on the RPA-coated 3′ ssDNA overhang and catalyzes strand invasion into a homologous DNA template.[6] The strand invasion event creates a D-loop, which is used as a primer for DNA synthesis. The extended strand can be dissociated from its template by a DNA helicase, or the Holliday junction can be processed with a DNA nuclease and ligase.[9]

Consistent with its central role in DSB repair, Mre11 and Rad50 orthologs can be found in all kingdoms of life.[14] However, in most bacteria, DSB resection is performed by the well-characterized

Received: February 5, 2011
Revised: May 6, 2011
Published: June 15, 2011

RecBCD complex,[15] rather than the bacterial MR complex (SbcC/D), which is considered a paralog of the eukaryotic MR and functions to prevent the replication of long palindromes that can form cruciform structures.[16] Bacteriophage T4 (T4) also contains Mre11 (gp47) and Rad50 (gp46) orthologs, and gene knockout experiments indicate that both Mre11 and Rad50 must be present for homologous recombination and DSB repair, suggesting that the physiological roles of eukaryotic and T4 MR complex are similar.[17,18]

Mre11 is a member of the protein phosphatase superfamily, which requires divalent metals for their activity.[19] *In vitro*, Mre11 from several sources have been shown to contain Mn^{2+}-dependent 3′ to 5′ dsDNA exonuclease and ssDNA endonuclease activities.[20−23] However, it is unclear if these are the physiologically relevant activities, as they appear to be incompatible with production of a 3′ ssDNA overhang. Interestingly, the replacement of the canonical metal cation, Mn^{2+}, with Mg^{2+} leads to an alteration in nuclease activity in T4 and *Pyrococcus furiosus* Mre11 (*Pfu*Mre11).[20,24] In both cases, Mg^{2+} promotes a dsDNA endonuclease activity, and in the case of *Pfu*Mre11, it was shown that the resulting product is an 3′ ssDNA overhang. In the T4 system, two recombination proteins, UvsY and gp32, increase the ability of Mre11 to utilize Mg^{2+} by ~10-fold.[20] The crystal structures of Mre11 from *Pfu*Mre11 (PDB: 3DSC) and *Thermotoga maritima* (*Tm*Mre11, PDB: 2Q8U) reveal a dimeric structure, and it is thought that the dimer is the physiologically relevant oligomeric form.[25,26] Dimeric *Pfu*Mre11 can simultaneously bind two blunt DNA ends or a single-branched dsDNA.[26] The *Pfu*MR complex is a heterotetramer ($Mre11_2/Rad50_2$),[27] and in at least the T4 system, the nuclease activity of Mre11 is highly dependent on Rad50.[20]

Rad50 is a member of the Structural Maintenance of Chromosomes (SMC) protein family, which are in turn members of the ATP Binding Cassette (ABC) protein superfamily.[28] The ABC protein superfamily is one of the largest and most highly conserved superfamilies known, and its members are found in large numbers in all organisms.[29] The common feature of ABC proteins is the nucleotide binding domain (NBD), which is dimeric and binds/hydrolyzes ATP at its dimeric interface.[30] By itself, T4 Rad50 is a relatively inefficient ATPase with a k_{cat} of 0.15 s^{-1} but is activated 22-fold upon binding Mre11 and DNA (separately Mre11 and DNA have little effect).[20] ATP hydrolysis is positively cooperative with Hill coefficients of 1.4 and 2.4 for Rad50 and the MR-D complex, respectively. ATP hydrolysis is not necessary for ssDNA endonuclease activity or for the exonucleolytic removal of the first nucleotide at the end of the DNA.[20] However, ATP hydrolysis enhances repetitive exonuclease activity, leading to the hypothesis that ATP hydrolysis drives translocation of the MR complex following nuclease activity and product release.

ABC proteins contain six conserved motifs that make up the NBD.[6] These consist of the Walker A motif containing the essential active site lysine,[7] the Walker B motif containing active site carboxylates,[7] the Q motif, the H-loop, the D-loop, and the Signature motif. All of the six motifs have been implicated in forming the complete ABC protein ATPase active site. A crystal structure of dimeric ATP-bound *Pfu*Rad50 shows a head-to-tail arrangement so that each subunit presents its conserved motifs at the dimeric interface (Figure 1A).[31] The Walker A, Walker B, Q-loop, and H-loop motifs from one monomer form one-half of the ATP binding site with the Signature and the D-loop motifs from the adjacent monomer completing the active site.[8] Rad50 proteins have an additional conserved motif, the CXXC motif that is located in the middle of a coiled-coil that splits the N- and

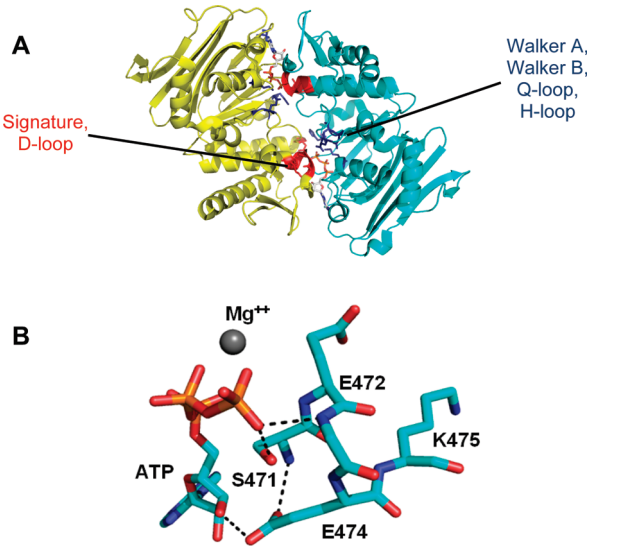

Figure 1. (A) Ribbon structure of the dimeric *Pfu*Rad50 NBD (PDB: 1F2U). The subunits of the dimer are colored yellow and cyan with the two ATP molecules located at the dimer interface colored in CPK. The Signature motif and D-loop from each subunit are colored in red and the Walker A, Walker B, Q-loop, and H-loop motifs are colored in blue. The coiled-coil domain is not present in the crystal structure. (B) A close-up of the Signature motif residues from the T4 homology model generated using the Swiss-model server[52] and based on 1F2U. ATP, Mg^{2+}, and the residues mutated in this study are noted. Dashes represent potential hydrogen bonds.

C-terminal subdomains of the NBD. The CXXC motif has been shown in dimerize with a second CXXC motif to bind a Zn^{2+} cation in a tetrathiolate linkage similar to zinc-finger proteins.[32] The exact function of this linkage is unclear, but it is thought to mediate Rad50-dependent tethering of DNA ends.[14]

As the defining feature of the ABC protein superfamily, the Signature motif (S·G/A·G·E/Q·K/R) has been the subject of intense investigation. However, its precise role in ATP hydrolysis and regulation still remains unclear.[29] As one of the two motifs that form the ATP active site *in trans*, it is thought that Signature motif residues are involved in the formation of the ATP-bound NBD dimer.[31,33] The Signature motif serine is positioned at the N-terminal end of a long α-helix (Figure 1A) and it has been proposed that the serine directs the positively charged dipole toward the γ-phosphate of ATP, thus counteracting the buildup of negative charge that occurs during the transition state.[31] It has also been proposed that an inward rotation of the Signature motif α-helix, which occurs upon ATP binding, is responsible for driving the large conformational changes that presumably occur during the ATP hydrolysis cycle.[28] These large conformational changes are thought to be involved in ATP cooperativity and possibly transmitted to the other associated functional domains (e.g., transmembrane domains for ABC transporters or Mre11 for Rad50).[31,34] To further reveal the functional importance of Rad50 Signature motif residues and evaluate their roles in the mechanism of ATP hydrolysis and regulation, we have individually mutated four of its five residues (the absolutely conserved glycine was not altered) and determined their effects on ATPase and Rad50-dependent Mre11 nuclease activities. All of the mutants display altered ATPase and/or nuclease activity to varying degrees (e.g., a 480-fold decrease in k_{cat}-ATP for S471M

and a 25-fold increase in K_m-ATP for E474Q). Mutation of the Signature motif residues Ser^{471}, Glu^{474}, and Lys^{475} reduces the level of DNA activation of ATPase activity, suggesting that these residues are involved in the allosteric transmission between the DNA and ATP binding sites. On the other hand, mutation of the noncanonical T4 Signature motif residue, Glu^{472}, has no effect on DNA activation. Mutation of Ser^{471} decreases ATP cooperativity to varying degrees depending on nature of the altered side chain, indicating that the signature motif is involved in communication between ATP sites. ATP hydrolysis is not necessary for exonuclease activity when the nuclease probe is located at the second position relative to the 3′ end of the DNA, but defects in ATP hydrolysis have substantial effects when the probe is placed at the 17th position, suggesting that ATP hydrolysis is more important for translocation of the complex than for Mre11 nuclease activity *per se*. Together, these data confirm the importance of the ABC protein Signature motif and demonstrate its role in ATP binding, hydrolysis, and cooperativity and in allosteric communication between the DNA and ATP binding sites of the MR complex.

MATERIALS AND METHODS

Materials. Oligodeoxynucleotides used for mutagenesis were purchased from either Integrated DNA Technologies or the Iowa State University DNA Facility. *Pfu* DNA polymerase Ultra was purchased from Agilent Technologies, Inc. DNA sequencing was performed at the Iowa State University DNA Facility. Isopropyl-β-D-thiogalactopyranoside (IPTG) was purchased from Gold Biotechnology. Sulfopropyl (SP) sepharose fast flow was purchased from GE Healthcare. Chitin Beads were purchased from New England Biolabs. Coupling enzymes (pyruvate kinase and lactate dehydrogenase), dNTPs, nicotinamide adenine dinucleotide (NADH), and nickel−agarose were purchased from Sigma-Aldrich Chemical Co. Phosphoenolpyruvate was purchased from Alfa Aesar. Adenosine 5′-triphosphate was purchased from USB Corp. Antibiotics were purchased from either USB Corp. (ampicillin) or Duchefa Biochemei (kanamycin). Chemicals, buffers, and media components were purchased from Fisher Scientific.

Subcloning of the T4 Rad50 Gene. The open reading frame encoding T4 Rad50 contains an intragenic NdeI site that was silently mutated using the Stratagene QuikChange site-directed mutagenesis protocol. The forward sequence of the mutagenic primer (NdeKO-F) can be found in Supporting Information Table S1. After confirming the mutation by DNA sequencing, the Rad50 open reading frame was amplified from gp46-pTYB1[20] using PCR primers Gp46-Nde-F and gp46-Bam-R (sequences in Table S1) and subcloned into the pET28b expression plasmid using standard molecular biology techniques.

Mutagenesis, Protein Expression, and Purification. The Stratagene QuikChange site-directed mutagenesis protocol was used to generate the desired mutations. The presence of the mutation and the integrity of the remaining coding sequence were verified by DNA sequencing. The forward primer sequences used in the mutagenic reactions can be found in Table S1.

Bacterial expression of Mre11 and Rad50 was carried out as previously described with the exception that the expression vector for Rad50 was gp46-pet28 rather than gp46-pTYB1. Purification of Mre11 was carried out as previously described.[20] Rad50 purification relied on a hexahistidine tag provided by the pet28 vector rather than the intein/chitin binding domain of the pTYB1 vector that was used previously.[20] Cell pellets containing expressed Rad50 (10 g wet cell paste) were resuspended in 100 mL of buffer containing 20 mM TRIS-Cl, 500 mM NaCl, 5 mM imidazole, and 10% glycerol at pH 8.0 (4 °C). Lysis was accomplished by passage thru an EmulsiFlex-C5 (Avestin, Inc.) at ∼16 kpsi. The lysate was clarified by centrifugation at ∼32 500*g* and the supernatant loaded onto ∼3 mL of Ni−agarose resin. The column was washed with 150 mL of lysis buffer, followed by 50 mL of lysis buffer containing 20 mM imidazole then 100 mL of lysis buffer containing 1 M NaCl. Prior to elution, the column was washed with 50 mL of 20 mM TRIS-Cl, 200 mM NaCl, and 10% glycerol at pH 8.0 (4 °C). The protein was eluted in buffer containing 20 mM TRIS-Cl, 200 mM NaCl, 150 mM imidazole, and 10% glycerol at pH 8.0 (4 °C). The fractions containing protein were pooled and loaded onto 10 mL of SP-sepharose equilibrated with 20 mM TRIS-Cl, 200 mM NaCl, and 10% glycerol at pH 8.0 (4 °C). The column was washed with 100 mL of equilibration buffer and eluted with 20 mM TRIS-Cl, 400 mM NaCl, and 20% glycerol at pH 8.0 (4 °C). The fractions containing protein were pooled, and the concentration was determined spectrophotometrically using an extinction coefficient (ε_{280} = 33 140 M^{-1} cm^{-1}) calculated from the deduced protein composition.

Steady-State ATPase Kinetics. For measurement of enzyme activity, a coupled enzyme assay was employed.[35,36] Initial velocities were determined by coupling the production of ADP to the oxidation of NADH with pyruvate kinase/lactate dehydrogenase (1.8 units PK, 3 units LDH/assay). All assays were done at 30 °C in the presence of 50 mM TRIS-Cl, 50 mM KCl, 5 mM $MgCl_2$, and 0.1 mg/mL BSA at pH 7.6 in a volume of 300 μL. Proteins were assayed fluorometrically using an excitation wavelength of 340 nm and monitoring the rate of change in NADH fluorescence (emission wavelength of 460 nm) on either a SLM-Aminco (SLM Instruments, Inc.) or a Cary Eclipse spectrofluorometer (Varian). All assays were started with the addition of Rad50. ATP concentrations used for each mutant varied from at least 5-fold above to at least 5 below the reported K_m-ATP values. For estimates of maximum velocity (V_{max}), Michaelis constant (K_m), and Hill coefficient, the reaction velocities at various ATP concentrations were fitted to the Hill equation

$$v = \frac{V_{max}[S]^n}{K_m{}^n + [S]^n} \quad (1)$$

using Sigmaplot 10.0/Enzyme Kinetics Module 1.3 (Systat Software, Inc.). An F-test was employed for the WT enzyme to justify fitting the data to a more complicated Hill model. Steady-state kinetic constants were determined for Rad50 and the Rad50/Mre11/DNA (MR-D) complex. The Mre11 concentration was always in slight excess over the Rad50 concentration. All MR-D assays contained an excess of DNA (at least 1.5-fold over protein complex) and well above the $K_{activation}$ for DNA (see below). The sequence of the oligonucleotides (ds50-F and ds50-R) used to create the DNA substrate can be found in Supporting Information Table S1.

Determination of the Activation Constant for DNA. The activation constant (K_{act}) for DNA was estimated by measuring the initial velocities of the MR complex at various DNA concentrations. These initial velocities, representing the average of three independent measurements, were fitted in Dynafit (Biokin, Ltd.)[37] to a simple bimolecular equilibrium mechanism.

The Rad50 and Mre11 concentrations were 10 and 13 nM, respectively. The buffer conditions were the same as that used in the steady-state kinetics. The ATP concentration was constant and saturating (320 μM).

Determination of the Equilibrium Dissociation Constant for ATP. All fluorescence measurements were performed using either a SLM-Aminco (SLM Instruments, Inc.) or a Cary Eclipse spectrofluorometer (Varian). Intrinsic tryptophan fluorescence of WT (0.5 and 1 μM), S471A (0.44 and 0.88 μM), S471R (0.5 and 0.8 μM), S471 M (1.15 μM), E472G (0.6 μM), E474Q (1.1 μM), and K475 M (1.0 μM) was measured at 30 °C in 3.0 mL 50 mM Tris-Cl, 50 mM KCl, and 10 mM $MgCl_2$ at pH 8.0. Samples were excited at 295 nm, and the emission was monitored at 335 nm. For data analysis, values measured at the fluorescent emission peak of 335 nm were corrected for dilution and ATP inner filter effect. The corrected fluorescence data were plotted against ATP concentrations and fit in Dynafit (Biokin, Ltd.)[37] to a simple bimolecular equilibrium mechanism. The K_d estimates reflect the average of at least three separate titrations.

Determination of Nuclease Activity. The product profile of MR complex nuclease activity was monitored using denaturing polyacrylamide gel electrophoresis (PAGE). All assays were done at 30 °C in the presence of 1 μM ^{32}P-DNA substrate (prepared as described in the Supporting Information), 50 mM TRIS-Cl, 50 mM KCl, 5 mM $MgCl_2$, 0.3 mM $MnCl_2$, and 0.1 mg/mL BSA at pH 7.6. The concentration of ATP was kept at 5× the K_m-ATP for each protein with the exception of the E474Q, which was held at 4× K_m-ATP. The reaction was started by addition of the DNA substrate solution (containing $MgCl_2$) to an equal volume of the protein solution (containing $MnCl_2$ and ATP). At times 0, 5, 10, and 20 min, an aliquot (10 μL) was removed and quenched with an equal volume of stop buffer containing 50% formamide/100 mM EDTA. The zero time point was taken prior to the initiation of the reaction by sequentially adding 5 μL of protein solution then 5 μL of the DNA substrate to the stop buffer. Reaction products were resolved with 16% denaturing PAGE containing 7.5 M urea in TBE buffer. Gels were run for 3−3.5 h at a constant power (60 W). The gel was exposed for 2 h to a PhosphorImager screen and visualized using a Typhoon PhosphorImager.

The exonuclease activity of the MR complex was also monitored using a real-time assay that detects activity by monitoring the liberation of an internal fluorescent 2-aminopurine (2-AP) deoxyribonucleotide.[38] The sequence of the oligonucleotides [ds50-F(3′2AP), ds50-R(3′2AP), ds50-F(3′17AP), ds50-R-(3′17AP)] used to create the nuclease substrates can be found in Table S1. All assays were done at 30 °C in the presence of 50 mM TRIS-Cl, 50 mM KCl, 5 mM $MgCl_2$, 0.3 mM $MnCl_2$, and 0.1 mg/mL BSA at pH 7.6. Samples were excited at 310 nm, and the rate of change in fluorescence at 375 nm was monitored. Initial rates were determined for the MR complex on the second position DNA substrate over a 5−10 min period in the absence of ATP. For the 17th position DNA substrate, rates were determined over the initial 5 min of the reaction for the MR complex in the absence and presence of ATP. The concentration of Mre11 was always in slight excess to Rad50 (0.95 ratio, Rad50:Mre11). The ATP independent nuclease rate was protein concentration dependent; thus, all assays were done at a single protein concentration (0.4 μM Rad50, 0.42 μM Mre11).

Oligomeric Determination of the T4 Rad50/Mre11 Complex. T4 Rad50 and Mre11 were combined in equal molar ratios and was exhaustively dialyzed against 2 L of 50 mM TRIS-Cl, 50 mM NaCl at pH 7.6 (4 °C). The final dialysate was used to dilute the protein samples to an absorbance at 280 nm of 0.4 and 0.6. Equilibrium 6-channel charcoal-filled Epon centerpieces were used with 120 μL of sample and 130 μL of the final dialysate as the reference in a Beckman Coulter Proteomelab XL-A analytical ultracentrifuge. Equilibrium at 4 °C was established at speeds of 11 300, 13 800, and 15 800 rpm. Concentration gradients were recorded at 280 nm beginning at 72 h for the initial velocity. Subsequent scans were recorded at 20 h (13 800 rpm) and 17 h (15 800 rpm) after the correct velocity had been achieved. An additional scan was taken 1 h after the initial scan at each velocity to ensure equilibrium had been established.

The data that were collected for WT and S471R (two concentrations at three speeds each) were simultaneously fit using SEDPHAT.[39] Global fits were accomplished with the Simplex algorithm. Molecular weight (MW) averages and standard errors were derived from a Monte Carlo simulation for nonlinear analysis with 500 iterations per fit and a confidence level of 0.9.

Table 1. Steady-State ATPase Kinetic and Mg·ATP Dissociation Constants for WT and Mutant Rad50 Proteins[a]

protein	K_m (μM)	k_{cat} (s^{-1})	n	K_d (μM)[b]
WT[c]	16 ± 1	0.145 ± 0.003	1.4 ± 0.1	9.4 ± 1.2
S471A	131 ± 8	0.113 ± 0.003	1.7 ± 0.1	100.8 ± 7.0
S471R	n.d.[d]	0.0018 ± 0.0002[e]	n.d.	4.1 ± 0.8
S471M	n.d.	0.0023 ± 0.0002[e]	n.d.	15.9 ± 1.0
E472G	4.4 ± 0.5	0.032 ± 0.001	1.1 ± 0.2	5.6 ± 1.0
E474Q	316 ± 13	0.20 ± 0.01	1.8 ± 0.1	196.1 ± 22.0
K475M	53 ± 1	0.035 ± 0.001	1.7 ± 0.2	29.2 ± 4.6

[a] Fluorometric assays were performed in 50 mM TRIS-Cl, 50 mM KCl, 0.1 mg/mL BSA (pH 7.6) in the presence of 5 mM $MgCl_2$ at 30 °C. Values determined by fitting data to a Hill equation. Errors represent the standard error of the fit. [b] Dissociation constants determined by tryptophan quenching using the same buffer conditions sans BSA. Values determined by fitting data to a multiple equilibrium model using Dynafit3 (Biokin[35]). Errors represent the standard error of the fit. [c] Herdendorf et al., JBC, 2011.[20] [d] n.d. indicates not determined. [e] Specific activity determination under standard conditions using the same buffer conditions. Error represents the standard deviation of four measurements.

RESULTS

Expression and Purification of Rad50 Signature Motif Mutants. WT T4 Rad50 was initially expressed using the pTYB1 vector and yielded a modest amount of soluble protein (~3 mg/L).[20] To improve the overall yield, the open reading frame was subcloned into the pET28b plasmid. The final yield of the N-terminal His_6 fusion protein following nickel affinity and cation exchange chromatography was ~20 mg protein per liter of LB. The WT and mutant proteins were purified to near homogeneity (Supporting Information Figure S1). The expression and purification of the WT T4Mre11 have been previously reported.[20]

Steady-State Kinetic Characterization of the ATPase Activity for WT and Mutant Rad50 Proteins. The data for WT Rad50 were originally fitted to both Michaelis−Menten and Hill equations. When comparing the sum of squares of the individual fits, the Hill equation yielded a smaller sum of squares.

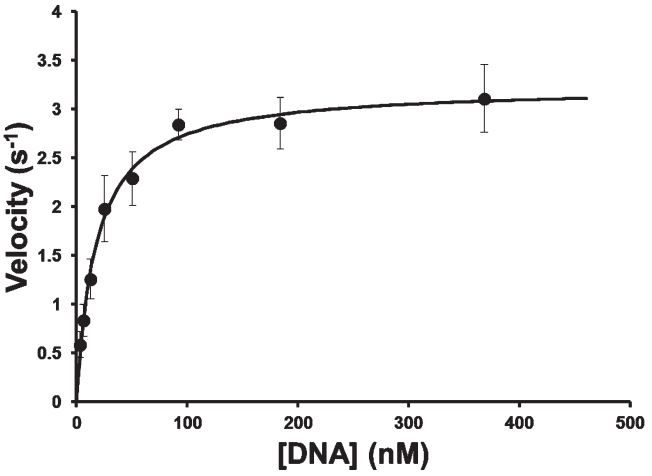

Figure 2. Activation constant (K_{act}) determination for DNA. Specific activity as a function of DNA concentration. Data points represent the average of three independent measurements. Each assay consisted of 10 nM WT Rad50, 13 nM WT Mre11 (buffer conditions described in the Methods section). ATP was kept constant and saturating (320 μM). Estimates of $K_{activation}$ (DNA concentration at half maximal velocity) and k_{cat} obtained by fitting data to a bimolecular equilibrium mechanism using DynaFit3 (biokin).[37]

This difference was less than 2-fold (1.5-fold); therefore, the fit statistics were compared using the more rigorous *F*-test.[40] The *F*-statistic at a *p* value of 0.01 with *degrees of freedom* of 1 (difference in the number of unknown variables in the two models under consideration) and 59 (number of data points minus the number of unknown variables) is 7.17. The calculated quotient ($df = 59$) is 22.76. On the basis of this result, the use of a more complicated Hill equation was deemed justified.

WT Rad50 has a k_{cat} of 0.145 s^{-1}, a K_m-ATP of 16 μM, and a Hill coefficient of 1.4 (Table 1). All of the Rad50 Signature motif mutants examined have altered kinetic constants (Table 1). S471A, E474Q, and K475 M have 8-, 20-, and 3.3-fold higher values for K_m-ATP, while E472G has a 3.6-fold lower value. Because of the extremely low ATPase activity of S471R and S471 M (80- and 60-fold decreases in k_{cat}-ATP, respectively), accurate values for K_m-ATP were unable to be determined, and therefore the k_{cat}-ATP values reported for these mutants are specific activities determined at saturating ATP concentrations. The ATP concentration was deemed saturating if the rate of ATP hydrolysis was unaffected by a 2-fold increase in its concentration and was at least 20-fold higher than the determined K_d-ATP (Table 1). The k_{cat}-ATP values for E472G and K475M are reduced by 4-fold compared to WT Rad50, whereas they are essentially unchanged for S471A and E474Q. The cooperativity of ATP hydrolysis for all mutants are relatively unaffected compared to the WT enzyme, given the standard error in the determination of this constant (Table 1). S471A, E474Q, and K475 M may be slightly more cooperative than WT and E472G may be less cooperative.

Mg·ATP Dissociation Constant Determination for WT and Mutant Rad50 Proteins. Considering that several of the Signature motif mutations resulted in an inflated K_m-ATP, Mg·ATP dissociation constants (K_d-ATP) were measured to determine if these increases are due to decreases in the affinity for Mg·ATP or a change in the kinetic mechanism for ATP hydrolysis. As seen in Table 1, the values for K_m- and K_d-ATP for WT and the mutant Rad50 proteins show a close correspondence with less than 2-fold differences between the determined constants. This suggests that T4 Rad50 follows a rapid-equilibrium kinetic mechanism for ATP hydrolysis and that K_m-ATP is a bona fide measure of ATP affinity.

Table 2. DNA Activation Constant for the Mre11/Rad50 Complex[a]

parameter	value
K_{act} (nM)[b]	17.7 ± 1.7
k_{cat} (s^{-1})[c]	3.2 ± 0.1

[a] DNA activation constant determined kinetically using the buffer conditions described in the Methods section. Values determined by fitting data to a bimolecular equilibrium model using Dynafit3 (Biokin). [b] DNA concentration at half maximal velocity. [c] Maximal velocity extrapolated to infinite DNA concentration.

DNA Activation Constant Determination for the WT MR Complex. Many ABC ATPases display an increase in ATPase activity in the presence of a secondary ligand (e.g., metabolite transported, DNA to be modified).[41−43] The ATPase activity of T4 Rad50 is also stimulated in the presence of Mre11 and DNA. To ensure the DNA concentration used in the MR-D assays was sufficient to produce the maximum activation, the steady-state activation constant was determined by measuring the velocity at various DNA concentrations. Since Mn^{2+} is not included in these assays, the exonuclease activity of Mre11 is negligible. Therefore, the DNA is not degraded and is considered an activator rather than a substrate. The data were fitted to a simple bimolecular equilibrium mechanism (Dynafit3, biokin[37]). The K_{act} for the WT MR complex is 17.7 nM, and the extrapolated k_{cat} (3.2 s^{-1}) is in good agreement with the value obtained when varying the concentration of ATP at a fixed DNA concentration (Figure 2 and Table 2). Because of the very high apparent affinity for DNA, it was not possible to determine the K_{act}-DNA for low activity mutants since the concentration of protein should not exceed the apparent K_{act}-DNA (i.e., the ATPase activity at protein concentrations in the range of 10 nM is difficult to accurately measure for the low-activity Rad50 mutants).

Steady-State Kinetic Characterization of the ATPase Activity for WT and Mutant MR-D Complexes. The addition of Mre11 to WT Rad50 (to form the MR complex) results in a 3-fold increase in K_m-ATP and no significant changes in the k_{cat} or Hill coefficient.[20] The addition of DNA to the MR complex (to form the MR-D complex) results in a 22-fold increase in k_{cat}, an increase in the Hill coefficient from 1.4 to 2.4, and no change in K_m-ATP.[20] On the basis of these changes, it was determined that a comparison of Rad50 to the MR-D complex would be the most informative since all three kinetic parameters are affected.

The 3-fold increase in K_m-ATP between Rad50 and the MR-D complex is essentially maintained in all of the Signature motif mutants (2.8−3.9-fold increases). In contrast, only the E472G mutant retains the 22-fold increase in k_{cat}-ATP. The k_{cat}-ATP of S471A, S471R, S471M, E474Q, and K475M is increased 6-, 8-, 2.5-, 10.5, and 6.3-fold upon binding of Mre11 and DNA. These differences are not due to decreases in DNA affinity since DNA was held at saturating concentrations (at least two concentrations of DNA were tested). The degree of cooperativity for ATP hydrolysis (Hill coefficient) is not significantly altered for E472G ($n = 2.0$), only slightly reduced in the S471A, E474Q, and K475 M ($n = 1.8−1.9$), moderately reduced in S471R ($n = 1.4$), and completely eliminated in S471 M ($n = 0.9$). The collected data and fitted curves

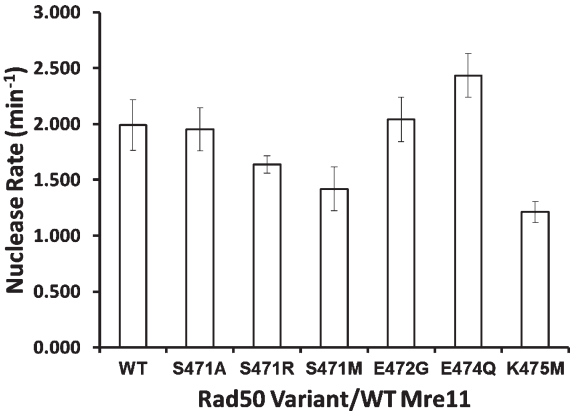

Figure 3. WT and mutant steady-state exonuclease activity on the second position DNA substrate. Exonuclease activity measured by the release of 2AP as a function of time. Each assay consisted of Rad50, Mre11, 1.2 μM DNA substrate, and 0.3 mM $MnCl_2$ (DNA substrate and buffer conditions described in Methods section). The 2AP probe is located at the second position relative to the 3′ end. Each specific activity estimate is an average of six measurements (three measurements at each of two protein concentrations, 50/100 nM Rad50 complexed with 53/105 nM Mre11). Error bars represent the standard deviation of the averaged values.

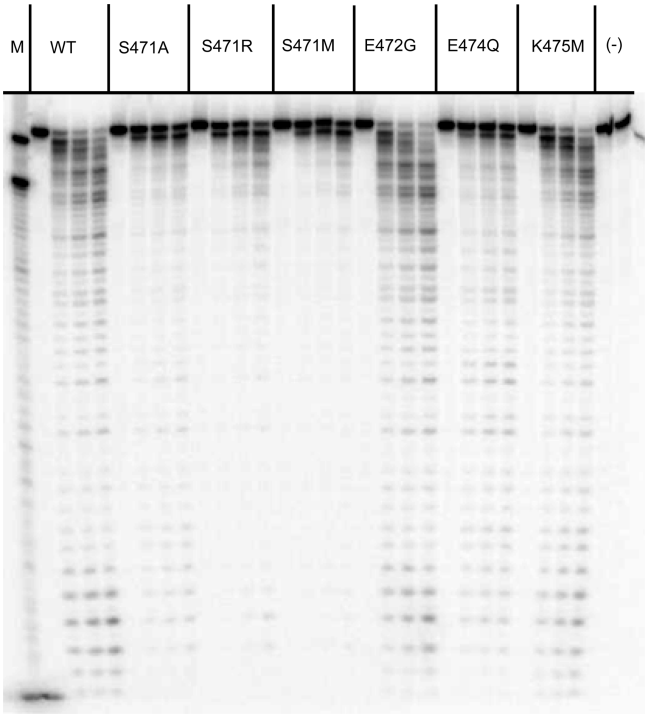

Figure 4. WT and mutant nuclease activity. Visualization of nuclease products using 16% Urea-PAGE is shown. The reactions were carried out at 30 °C, and the time points for each protein are 0, 5, 10, and 20 min. Each assay consisted of 400 nM Rad50, 420 nM Mre11, 1 μM DNA substrate, 0.3 mM $MnCl_2$ (DNA substrate and buffer conditions described in Methods section). The concentration of ATP was 5-fold above the K_m, with the exception of E474Q (4× K_m) The final two lanes are a no protein control with time points of 0 and 20 min. Lane 1 contains a 49- and 40-mer marker.

for WT and the two lowest activity mutants (S471R and S471M) are shown in Supporting Information Figure S2.

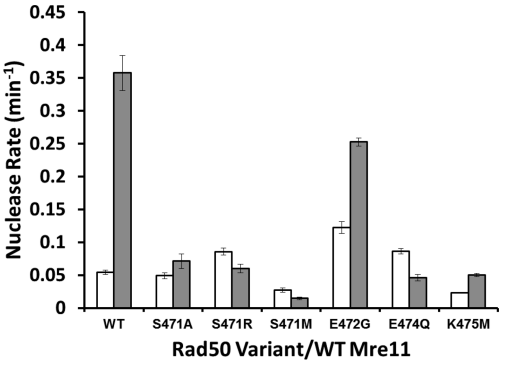

Figure 5. WT and mutant steady-state exonuclease activity on the 17th position DNA substrate. Exonuclease activity measured by the release of 2AP as a function of time. Each assay consisted of 400 nM Rad50, 420 nM Mre11, 1.3 μM DNA substrate, and 0.3 mM $MnCl_2$ (DNA substrate and buffer conditions described in Methods section): open bars (−) ATP; shaded bars (+) ATP). The concentration of ATP, when included, was kept constant and at least 4-fold above the K_m. The 2AP probe is located at the 17th position relative to the 3′ end. Each specific activity estimate is an average of three measurements. Error bars represent the standard deviation of the averaged values.

Nuclease Activity of the WT and Mutant MR-D Complexes.

The primary nuclease activity of Mre11 is a 3′ to 5′ exonuclease, which is highly dependent on complex formation with Rad50.[20] To ensure that the mutant Rad50 proteins bound both Mre11 and DNA normally, the ATP-independent 3′ to 5′ exonuclease activity was followed by the liberation of the fluorescent nucleotide analogue 2AP located in the second position relative to the 3′ end of the 50 bp DNA substrate. Since this assay is performed without ATP, it is expected that mutations in the ATP binding site of Rad50 will have little effect on the exonuclease activity of the MR complex. Consistent with this, none of the Signature motif mutations greatly alter the exonuclease rate when the 2-AP is located at the second position (1.4−2.4 min^{-1}, Figure 3), indicating that neither DNA nor Mre11 affinity is substantially altered by the Signature motif mutations.

Next, the ATP-dependent nuclease activity of the MR complex mutants was assayed using denaturing PAGE. The standard 50 bp dsDNA substrate was used where the 5′ end of ds50-F was labeled with ^{32}P and ds50-R contained a phosphorothioate linkage between the first and second positions (relative to the 3′ end) to prevent the exonuclease activity from degrading both strands. This assay was carried out over a time period of 30 min and therefore should not be considered a true steady-state reaction. As shown in Figure 4, using this dsDNA substrate the nuclease activity of the MR complex produces a broad range of products ranging from 49 to ∼5 nucleotides in length. The appearance of short DNA products at even the earliest time point suggests moderate processivity. WT, E472G, and K475M show the highest levels of nuclease activity, S471A and E474Q have intermediate levels, and S471R and S471M have the lowest levels with S471R having slightly more than S471M.

To quantitate the differences in ATP-dependent nuclease activity between WT and the Signature motif mutants, the real-time 2AP fluorescent assay was again employed, but with the probe located in the 17th position rather than the second position (Figure 5). The nuclease activity using the 17th position substrate is ATP dependent and therefore is likely to be affected by the Signature motif mutations.[20] The initial rates are collected

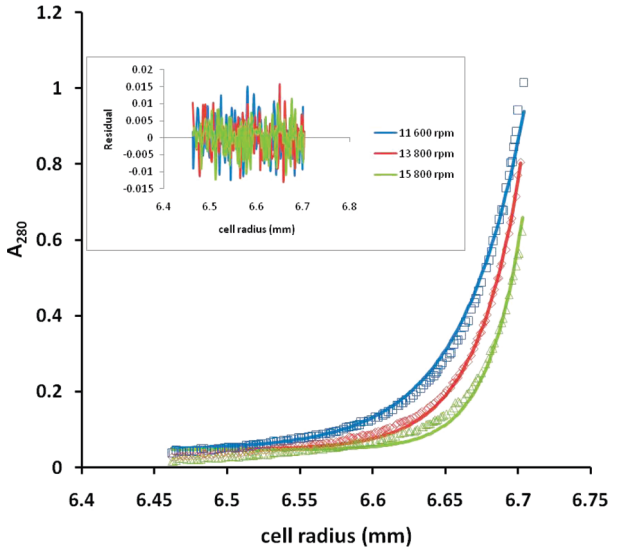

Figure 6. Oligomeric determination of the WT MR complex. Representative analytical sedimentation equilibrium ultracentrifugation results for one complex concentration (WT, initial A_{280}: 0.6). Equilibrium concentration gradients formed at velocities of 11 600 (□), 13 800 (◇), and 15 800 rpm (○). Solid lines represent the global fits produced. Inset: fit residuals.

over the first 5 min of the reaction and therefore approximate steady-state conditions. This 3′ to 5′ exonuclease assay indicates that all of the Signature motif mutations result in decreased ATP-dependent nuclease activity when compared to WT. The nuclease activity of E472G is only slightly reduced compared to WT (1.4-fold), whereas all other mutants are reduced by at least 5-fold. The nuclease rates of S471A and K475 M are reduced by 5- and 6-fold, respectively, but maintain some level of ATP activation. S471R, S471M, and E474Q also have significantly reduced nuclease rates (6-, 18-, and 7-fold, respectively) and are inhibited rather than activated by the presence ATP. Consistent with what was observed with the second position 2AP substrate, in the absence of ATP the exonuclease rates for the signature motif mutants with the 17th position 2AP substrate were all within 2.5-fold of the WT value, again indicating Mre11 and DNA binding affinity is unaffected.

Oligomeric Determination of the WT and S471R MR Complexes. Although it has been presumed that the T4 MR complex is a heterotetramer ($Mre11_2/Rad50_2$) in solution, there has not been direct evidence for this. To determine the oligomeric state of the MR complex, sedimentation equilibrium analytical ultracentrifugation (AUC) was performed. Sedimentation equilibrium AUC provides a thermodynamically rigorous measurement of the average molecular weight of a protein as a function of its concentration. Data exhibiting concentration gradients of the WT MR complex at 4 °C were analyzed as a single species. Monte Carlo simulations yield MW estimates that range from 195 496 to 210 911 Da (Table 4). These data suggest the T4 MR complex is a heterotetramer in solution (deduced MW is 205 568). Fit residuals were small and well dispersed (Figure 6). Mutation of the *Pfu*Rad50 Signature motif serine to arginine (within the context of the NBD only) abrogates dimerization.[44] Although their ATP affinities strongly suggest that S471R and S471 M are dimeric, we used sedimentation equilibrium AUC to determine the oligomeric state of the S471R MR complex (since a loss of Rad50 dimerization could explain its large reduction in k_{cat}-ATP). Fitting the data in an identical fashion as the WT MR complex yielded MW estimates from 208 152 to 218 592 Da, values indicative of a heterotetramer. The standard error of the fit was higher for the S471R MR complex (4.1 and 5.2%) as compared to WT (0.6 and 0.8%), which appears to be due to the presence of a minor amount of a higher MW component that was only present in the S471R MR complex sample. Since the purity of WT and S471R is essentially identical (as judged by SDS-PAGE, Supporting Information Figure S1), it is likely that this higher MW component represents a minor fraction of soluble aggregate.

DISCUSSION

One of the defining features of the ABC protein superfamily is the Signature motif (S·G/A·G·E/Q·K/R). The crystal structure of *Pfu*Rad50 reveals that the Signature motif is part of a shared dimeric active site where the Walker A and B, Q- and H-loop motifs from one monomer combine with the Signature and D-loop motifs of the other monomer to complete an ATP binding and hydrolysis site.[31] Although it is clear that the Signature motif is crucial to the function of ABC proteins, its roles in ATP binding, hydrolysis, and regulation are poorly understood.[29,45] Highlighting the importance of this motif is the fact that six different Signature motif mutations have been identified in the human ABC protein superfamily member, cystic fibrosis conductance regulator (CFTR).[46] These mutations result in cystic fibrosis and cover four out of the five Signature motif residues (S549R, S549I, S549N, G551S, G551D, Q552 K, R553G, and R553Q). The function of the Signature motif and the deleterious nature of these mutations have just begun to be explored.

Most members of the ABC superfamily are associated with transmembrane domains and are therefore challenging to biochemically characterize in an *in vitro* system.[30] The common solution to this problem has been to investigate the isolated NBD of the ABC protein. These systems, although incomplete, have led to a great number of insights related to the mechanism of ATP hydrolysis, but they are unable to evaluate the allosteric regulation that likely occurs in a fully functioning system.[47−50] Rad50 contains a prototypical ABC protein NBD, along with a coiled-coil domain that is required for the binding of Mre11.[14] Expression and purification of full-length Rad50 from *S. cerevisiae* or human are difficult, and only microgram quantities of protein are obtained.[22,51] Additionally, current protocols for eukaryotic Rad50 expression require coexpression of Mre11, which presumably improves the stability and/or solubility of the expressed protein.[51] Once formed, the MR complex is stable and is not easily separated, preventing a comparison of the properties of Rad50 alone to those of the MR complex. Similar to eukaryotic Rad50, full-length *Pfu*Rad50 is coexpressed with Mre11 and is subject to the same difficulties described for the eukaryotic proteins.[21] The coiled-coil domain of eukaryotic and archaea Rad50 contains over 900 and 600 amino acids, respectively, and this is the main source of their poor expression (Herdendorf, Parrott, and Nelson, unpublished observations). In contrast, the coiled-coil domain of T4 Rad50 is made up of just 200 amino acids, and T4 Rad50 is easily expressed and purified in its fully active form.[20] Importantly, the NBDs of phage, eukaryotic, and archaea Rad50 are nearly identical in size, and the six ABC motifs are well conserved, which enabled the creation of a T4 structural homology model using the Swiss-Model server.[52] We have recently biochemically characterized the nuclease and ATPase

Table 3. Steady-State ATPase Kinetic Constants for WT and Mutant Rad50s Complexed with Mre11 and DNA[a]

protein	K_m (μM)	k_{cat} (s^{-1})	DNA activation[b]	n
WT[c]	49 ± 2	3.2 ± 0.1	22	2.4 ± 0.2
S471A	500 ± 53	0.64 ± 0.03	6	1.8 ± 0.2
S471R	22 ± 2	0.0146 ± 0.0004	8	1.4 ± 0.2
S471M	126 ± 13	0.0066 ± 0.0002	2.5	0.9 ± 0.1
E472G	13.3 ± 0.1	0.71 ± 0.01	22	2.0 ± 0.2
E474Q[c]	1253 ± 186	2.1 ± 0.2	10.5	1.8 ± 0.3
K475M	146 ± 14	0.221 ± 0.009	6.3	1.9 ± 0.3

[a] Fluorometric assays were performed in 50 mM TRIS-Cl, 50 mM KCl, 0.1 mg/mL BSA (pH 7.6) in the presence of 5 mM $MgCl_2$ at 30 °C. Values determined by fitting data to a Hill equation. Errors represent the standard error of the fit. [b] Fold increase in k_{cat} between MR-D and Rad50 (Table 1). [c] Herdendorf et al., JBC, 2011.[20] [c] Assay contained 10 mM $MgCl_2$.

Table 4. Sedimentation Equilibrium Centrifugation Results for WT and S471R MR Complexes[a,b]

protein	initial A_{280}	MW (Da)
WT	0.6	210911 ± 1294
	0.4	195496 ± 1548
S471R	0.6	218592 ± 11380
	0.4	208152 ± 8433

[a] Deduced MW for $(Rad50)_2/(Mre11)_2$ is 205 568 Da. [b] Analysis performed using the Sedphat software and fit to a single species model. Global fits were accomplished with the fitting algorithm. MW estimates and standard errors were derived from a Monte Carlo simulation for nonlinear analysis (500 iterations, confidence level: 0.9).

activities of T4 Rad50, the MR complex, and the MR-D complex.[20] We now use the T4 model system to evaluate the functional roles of the ABC protein Signature motif within the context of Rad50 alone or as the MR-D complex.

Role of the Signature Motif in ATP Hydrolysis. The Signature motif serine to arginine mutation has been previously made in *Pfu* (S793R), *S. cerevisiae* (S1205R), and human (S1202R) Rad50 proteins.[44,45] The mutation within the context of the NBD of *Pfu*Rad50 prevents ATP-dependent dimerization and abrogates binding of the fluorescent ATP analogue BODIPY FL AMP-PNP.[44] Full-length S793R was coexpressed with *Pfu*Mre11, and a qualitative examination indicated that its ATPase activity was substantially reduced.[45] An ATPase time-course was performed with the *S. cerevisiae* and human Rad50 mutants, but the kinetic parameters were not determined.[45] Unexpectedly, the S1202R mutation appears to increase the activity of human Rad50, whereas the S1205R mutation has no effect on *S. cerevisiae* Rad50. In the T4 Rad50 protein, we find that the S471R mutation causes 80- and 219-fold decreases in k_{cat}-ATP when compared to Rad50 or the MR-D complex, respectively, a 2.3-fold decrease in K_d-ATP when compared to Rad50, and 2.2-fold decrease in K_m-ATP when compared the MR-DNA complex (Tables 1 and 3).

Replacement of serine with the substantially longer side chain of arginine increased the enzyme's affinity for ATP. This result, combined with the large decrease in k_{cat}-ATP, suggests that there is an electrostatic attraction between the guanidinium group of Arg and the γ-phosphate of ATP, but in forming the interaction the γ-phosphate must move out of a position that is optimal for ATP hydrolysis. To test this hypothesis, we constructed S471M, which should be as sterically disruptive as S471R but lack the putative electrostatic interaction. Consistent with the hypothesis, we found that the S471M mutation resulted in a similar reduction in k_{cat}-ATP, but unlike S471R, the mutant had lower affinity for ATP compared to the WT enzyme.

The S471R mutant was chosen because it is one of the naturally occurring disease mutations in the CFTR gene.[46] However, a more appropriate assessment of the contribution of Ser^{471} to ATP binding and hydrolysis can be made by examining the more conservative S471A mutation. As expected, the effects of this mutation on k_{cat}-ATP are much less than the S471 M and S471R mutations. On the other hand, the K_m- and K_d-ATP increased ~10-fold, indicating weaker binding of ATP to the active site. The most striking feature of the S471A mutation is the reduction in DNA-activation from 22-fold for the WT MR-D complex to 6-fold for the S471A MR-D complex. Reductions of 2.5- and 8-fold are also seen for the S471M MR-D and S471R MR-D complexes, respectively. In the case of S471A, the decrease in DNA activation is due to the nearly normal k_{cat}-ATP when Mre11 and DNA are absent but a 5-fold decrease when they are present (compared to WT MR-D). In contrast to the k_{cat}-ATP, the fold change in K_m-ATP compared to WT is nearly equivalent for both S471A Rad50 and the S471A MR-D complex. This suggests that the interaction between the Signature motif serine and the γ-phosphate of ATP is present, and of equal strength, in both Rad50 and the MR-D complex, but binding of Mre11 and DNA to Rad50 induces a movement of Ser^{471} that repositions the γ-phosphate of ATP into a more optimal orientation for catalysis. Another notable feature of the Ser^{471} mutations is the observed reduction in ATP cooperativity (Hill coefficient). The MR-D complexes for S471M, S471R, and S471A have Hill coefficients of 0.9, 1.4, and 1.8, respectively, compared to 2.4 for the WT MR-D complex. This indicates that the communication between ATP binding sites within the Rad50 oligomer has been somehow altered. The Signature motif is located at the end of a long α-helix that, according to the crystal structures of *Pfu*Rad50 NBD, undergoes a substantial conformational change upon binding of ATP to its active site.[28,31,34] The Signature motif α-helix is connected via a short loop to a β-strand that contains the Walker B residues that form part of the other ATP active site. While the Walker B residues only slightly change positions in the ATP-free and ATP-bound forms of the *Pfu*Rad50 NBD structure (1F2U compared to 1F2T, 1.3 Å for the Walker B glutamate), it is possible that a more substantial conformational change occurs within the context of the MR-D complex. Indeed, the cooperativity of Rad50 ATP hydrolysis is significantly greater in the presence of Mre11 and DNA.

T4 Rad50 has a noncanonical residue (Glu^{472}) following the Signature motif serine, whereas most ABC proteins contain a glycine at this position. The original homology model of T4 Rad50 placed the carboxylic acid of Glu^{472} near the Mg^{2+} cation, so we hypothesized that they may electrostatically interact. However, our experimental data suggest that this is probably not the case. Although the k_{cat}-ATP for E472G has decreased by 4-fold (MR-D complex), the mutant has a 3.5-fold improved ATP affinity, which is inconsistent with the loss of a glutamate−Mg^{2+} interaction. On the basis of these results, we surmised that the placement of the Glu^{472} side chain in the original homology model (which was automatically generated by Swiss model[52]) was incorrect. Therefore, we sought to improve the homology model. To do this, we used the crystal structure of the *D. radiodurans* RecF protein, which is an ABC protein containing an arginine rather than a glycine residue following the Signature motif serine.[53] Additionally, RecF from several other species contain either a glutamate or a glutamine at this position. In

the *D. radiodurans* RecF structure, instead of the arginine guanidinium group being oriented toward the ATP active site, it is facing the opposite direction toward the C-terminal end of the α-helix.[53] To match the position of the RecF arginine, we manually rotated the Glu^{472} side chain in the T4 homology model about the β- and γ-carbons. The altered position of the Glu^{472} side chain in the homology model may provide an explanation for the source of the K_m-ATP and k_{cat} effects we observe upon its mutation to glycine. The carboxylic acid of Glu^{472} is now within 3.4 Å of the ε-amino group of Lys^{62} from the opposing monomer. Lys^{62} is located in the analogous position as the "R-loop" arginine that interacts with the α-phosphate of ATP in the crystal structure of *Pfu*SMC protein.[54] Based on these positions, loss of the Glu^{472}—Lys^{62} interaction may strengthen the ability of Lys^{62} to interact with the α-phosphate of ATP (lowering K_m-ATP), but alter the position of ATP (reducing k_{cat}-ATP).

The large inflation in the K_m- and K_d-ATP for the E474Q mutant (~20-fold) is somewhat surprising given that glutamine is a conservative substitution and is the naturally occurring residue in many ABC proteins, including most ABC transporters.[30] In the T4 homology model (Figure 1B), Glu^{474} forms hydrogen bonds with both the ATP ribose 3′ hydroxyl and the backbone amide of Ser^{471}. The E474Q mutation should allow for at least one of the hydrogen bonds to be maintained, albeit in a slightly weaker form due to the loss of ionic character. Loss of the other hydrogen bond by replacement of a proton-accepting with a protein-donating group may result in a slight steric clash that requires a movement of either the ATP ribose or Ser^{471} (depending on the orientation of side-chain amide). Either of these possibilities would produce the larger than expected decrease in ATP binding affinity that is observed. As mentioned above, many ABC proteins have a Gln at this position, including both *S. cerevisiae* and human Rad50. Our data predict that these proteins should have weaker affinity for ATP, which appears to be the case as the K_m-ATP's for the *S. cerevisiae*, and human MR complexes are 230 and 317 μM, respectively.[45]

On the basis of a very recent crystal structure of the *Pfu*Rad50 NBD,[34] it appears that Lys^{475} (Arg^{797} in *Pfu*Rad50) likely is involved in communication with Mre11 through an interaction with what has been termed the "signature coupling helix". The signature coupling helix controls the position of the Rad50 coiled-coil domain, which directly interacts with Mre11. The reduction in DNA activation (which requires the presence of Mre11) and in the Hill coefficient is consistent with altered Rad50-Mre11 communication. The reduction in k_{cat}-ATP in the K475 M mutant can also be understood in terms of a destabilization of the Signature loop due to loss of the interaction between Lys^{475} and the signature coupling helix.

Role of the Signature Motif in Mre11 Nuclease Activity. Relating the exonuclease activity of each mutant to its steady-state ATPase activity does not appear straightforward. Although it is clear that a decrease in ATPase activity affects exonuclease activity, the correlation is not direct and appears to be positionally specific. For example, while the ATPase activity of E472G is 4.6-fold lower than WT, its exonuclease activity is only 1.4-fold lower. The opposite relationship is seen with the E474Q mutant, where its ATPase activity is only 1.5-fold lower than WT but its exonuclease activity is 8.5-fold lower. Additionally, both the S471A and E472G MR-D complexes have similar ATPase activities, but very different exonuclease activities. It is highly likely that these varying affects arise from the fact that although the rate of ATP hydrolysis directly governs the nuclease/translocation rate,[20] the steady-state exonuclease reaction is not a direct reporter of that rate. Our previous work has shown that the rate-limiting step of the steady-state nuclease reaction appears to be the productive assembly of the complex.[20] Because of this situation, as long as k_{cat}-ATP is much greater than the steady-state exonuclease rate, the steady-state exonuclease rate represents a combination of the productive DNA binding rate and the number of binding events required to reach the nuclease probe position (i.e., processivity).

The k_{cat}-ATP values for S471A, K475M, and E474Q are well above their respective steady-state exonuclease rates, suggesting that their intrinsic nuclease/translocation rate should not directly contribute their steady-state exonuclease rates. Therefore, for these mutants, changes in ATP-dependent steady-state exonuclease rates likely reflect changes in their ability to initiate 3′ to 5′ exonuclease activity in the presence of ATP or in their processivity. The gel shown in Figure 4 suggests that S471A and E474Q appear have a reduced initiation rate (i.e., a slower appearance of the 49 nt product). This also appears to be the case for S471R and S471M. However, on the basis of the reduction in DNA products less than 49 nucleotides, it would appear that the S471R and S471 M mutant MR complexes are also defective in removing additional nucleotides. For these two mutants, which have severely reduced k_{cat}-ATP values, it is likely that the intrinsic rate of exonuclease/translocation has become rate-limiting. For both S471R and S471M, the exonuclease rates in the presence of ATP are slower than in its absence (Figure 5). This phenomenon was also observed in for the Walker A lysine mutant (K42M) with ATP and the WT MR complex when the nonhydrolyzable ATP analogue, AMP-PNP, is substituted for ATP.[20] The simplest explanation for this inhibition is that, following nuclease activity and dNMP release, the MR complex is stalled in the ATP-bound form and cannot translocate until hydrolysis occurs. In the absence of ATP, the complex dissociates from the DNA following nuclease activity and product release, allowing the complex to rebind to the DNA substrate in the $n + 1$ position (i.e., nonprocessive translocation). This stalling mechanism is consistent with the relatively unchanging product profile that is seen in the gel assay. The majority of the 49 nt product is produced during the first 5 min time point, and only a small increase is observed over the next 15 min.

Understanding the effects of the K475 M mutation on its nuclease activity is complicated by the discrepancy between the activities observed using the fluorometric or gel-based assays. With the exception of K475M, the results from the fluorometric assay correspond with the gel-based assay. However, for K475M, we have consistently observed a ~7-fold decrease in nuclease activity with the fluorometric assay but only slightly reduced activity with the gel-based assay. The source of this discrepancy is unclear, although it is reproducible. The fluorometric assay is more consistent with the reduction in k_{cat}-ATP, as are the *in vivo* experiments using the *S. pombe* system that demonstrate the mutation of the lysine residue corresponding T4 Lys^{475} results in sensitivity to camptothecin.[34] The two assays we have performed do not monitor identical activities. The fluorometric assay strictly measures exonuclease activity (i.e., production of free 2AP nucleotide), whereas the gel-based assay is capable of monitoring both exo and endonuclease activity. In the absence of gp32 and UvsY, the endonuclease activity of the WT complex appears to be negligible,[20] and the product profile generated in the K475M reaction appears to be normal; however, it may be possible that the K475M mutant has somehow affected this property. A resolution to this puzzling observation will likely require further exploration of the K475M mutant and the development of

additional nuclease assays that are capable of isolating the various potential nuclease activities of the MR complex.

Conclusions. The data presented here suggest specific roles for the T4 Signature motif residues in ATP affinity and the catalytic mechanism of ATP hydrolysis, which can likely be generalized to other ABC protein superfamily members. Additionally, comparison of the kinetic and thermodynamic parameters of the Signature motif mutants between Rad50 alone and the MR-D complex has revealed that the Signature motif is involved in the allosteric communication that occurs throughout the MR complex. These effects can be seen by the alterations in ATP cooperativity, DNA activation of ATP hydrolysis, and the effects on the ATP-dependent nuclease activity of Mre11. While it is possible that these effects are specific to Rad50 and Mre11, it is tempting to speculate that the Signature motif from other ABC proteins are involved in allosteric communication between their ATP active sites and other associated domains or heterologous proteins that are specific for each system (e.g., the transmembrane domain of ABC transporters).

■ ASSOCIATED CONTENT

Supporting Information. Experimental details, Table S1, and Figures S1 and S2. This material is available free of charge via the Internet at http://pubs.acs.org.

■ AUTHOR INFORMATION

Corresponding Author

*E-mail: swn@iastate.edu; Ph: 515-294-3434; Fax: 515-294-0453.

Funding Sources

This work was financially supported by The Roy J. Carver Charitable Trust and Iowa State University.

■ ABBREVIATIONS

DSB, double-strand breaks; HR, homologous recombination; NHEJ, nonhomologous end-joining; MMEJ, microhomology-mediated end-joining; MR, Mre11/Rad50; ssDNA, single-stranded DNA; T4, Bacteriophage T4; dsDNA, double-stranded DNA; *Pfu*, *Pyrococcus furiosus*; *Tm*, *Thermotoga maritime*; SMC, structural maintenance of chromosomes; NMD, nucleotide binding domain; SP, sulfopropyl; WT, wild-type; kan, kanamycin; amp, ampicillin; CBD, chitin binding domain; MR-D, Mre11/Rad50/DNA; 2-AP, 2- aminopurine; AUC, analytical ultracentrifugation; MW, average molecular weight; CFTR, cystic fibrosis conductance regulator.

■ REFERENCES

(1) Povirk, L. F. (2006) Biochemical mechanisms of chromosomal translocations resulting from DNA double-strand breaks. *DNA Repair 5*, 1199–1212.

(2) Bassing, C. H., and Alt, F. W. (2004) The cellular response to general and programmed DNA double strand breaks. *DNA Repair 3*, 781–796.

(3) McVey, M., and Lee, S. E. (2008) MMEJ repair of double-strand breaks (director's cut): deleted sequences and alternative endings. *Trends Genet. 24*, 529–538.

(4) Paull, T. T. (2010) Making the best of the loose ends: Mre11/Rad50 complexes and Sae2 promote DNA double-strand break resection. *DNA Repair 9*, 1283–1291.

(5) Daley, J. M., Palmbos, P. L., Wu, D., and Wilson, T. E. (2005) Nonhomologous end joining in yeast. *Annu. Rev. Genet. 39*, 431–451.

(6) Symington, L. S. (2002) Role of RAD52 epistasis group genes in homologous recombination and double-strand break repair. *Microbiol. Mol. Biol. Rev. 66*, 630–670.

(7) Wyman, C., and Kanaar, R. (2006) DNA double-strand break repair: all's well that ends well. *Annu. Rev. Genet. 40*, 363–383.

(8) Shrivastav, M., De Haro, L. P., and Nickoloff, J. A. (2008) Regulation of DNA double-strand break repair pathway choice. *Cell Res. 18*, 134–147.

(9) Krogh, B. O., and Symington, L. S. (2004) Recombination proteins in yeast. *Annu. Rev. Genet. 38*, 233–271.

(10) Mimitou, E. P., and Symington, L. S. (2009) DNA end resection: many nucleases make light work. *DNA Repair 8*, 983–995.

(11) Mimitou, E. P., and Symington, L. S. (2008) Sae2, Exo1 and Sgs1 collaborate in DNA double-strand break processing. *Nature 455*, 770–774.

(12) Niu, H., Chung, W.-H., Zhu, Z., Kwon, Y., Zhao, W., Chi, P., Prakash, R., Seong, C., Liu, D., Lu, L., Ira, G., and Sung, P. (2010) Mechanism of the ATP-dependent DNA end-resection machinery from Saccharomyces cerevisiae. *Nature 467*, 108–111.

(13) Zhu, Z., Chung, W., Shim, E., Lee, S., and Ira, G. (2008) Sgs1 Helicase and Two Nucleases Dna2 and Exo1 Resect DNA Double-Strand Break Ends. *Cell 134*, 981–994.

(14) Connelly, J. C., and Leach, D. R. F. (2002) Tethering on the brink: the evolutionarily conserved Mre11-Rad50 complex. *Trends Biochem. Sci. 27*, 410–418.

(15) Dillingham, M. S., and Kowalczykowski, S. C. (2008) RecBCD enzyme and the repair of double-stranded DNA breaks. *Microbiol. Mol. Biol. Rev. 72*, 642–671.

(16) Connelly, J. C., de Leau, E. S., and Leach, D. R. (1999) DNA cleavage and degradation by the SbcCD protein complex from Escherichia coli. *Nucleic Acids Res. 27*, 1039–1046.

(17) Mickelson, C., and Wiberg, J. S. (1981) Membrane-associated DNase activity controlled by genes 46 and 47 of bacteriophage T4D and elevated DNase activity associated with the T4 das mutation. *J. Virol. 40*, 65–77.

(18) Woodworth, D. L., and Kreuzer, K. N. (1996) Bacteriophage T4 mutants hypersensitive to an antitumor agent that induces topoisomerase-DNA cleavage complexes. *Genetics 143*, 1081–1090.

(19) Barford, D., Das, A. K., and Egloff, M. P. (1998) The structure and mechanism of protein phosphatases: insights into catalysis and regulation. *Annu. Rev. Biophys. Biomol. Struct. 27*, 133–164.

(20) Herdendorf, T. J., Albrecht, D. W., Benkovic, S. J., and Nelson, S. W. (2011) Biochemical characterization of bacteriophage T4Mre11/Rad50 complex. *J. Biol. Chem. 286*, 2382–2392.

(21) Hopfner, K. P., Karcher, A., Shin, D., Fairley, C., Tainer, J. A., and Carney, J. P. (2000) Mre11 and Rad50 from Pyrococcus furiosus: cloning and biochemical characterization reveal an evolutionarily conserved multiprotein machine. *J. Bacteriol. 182*, 6036–6041.

(22) Trujillo, K. M., and Sung, P. (2001) DNA structure-specific nuclease activities in the Saccharomyces cerevisiae Rad50*Mre11 complex. *J. Biol. Chem. 276*, 35458–35464.

(23) Trujillo, K. M., Yuan, S. S., Lee, E. Y., and Sung, P. (1998) Nuclease activities in a complex of human recombination and DNA repair factors Rad50, Mre11, and p95. *J. Biol. Chem. 273*, 21447–21450.

(24) Hopkins, B. B., and Paull, T. T. (2008) the p. furiosus mre11/rad50 complex promotes 5′ strand resection at a DNA double-strand break. *Cell 135*, 250–260.

(25) Das, D., Moiani, D., Axelrod, H. L., Miller, M. D., McMullan, D., Jin, K. K., Abdubek, P., Astakhova, T., Burra, P., Carlton, D., Chiu, H.-J., Clayton, T., Deller, M. C., Duan, L., Ernst, D., Feuerhelm, J., Grant, J. C., Grzechnik, A., Grzechnik, S. K., Han, G. W., Jaroszewski, L., Klock, H. E., Knuth, M. W., Kozbial, P., Krishna, S. S., Kumar, A., Marciano, D., Morse, A. T., Nigoghossian, E., Okach, L., Paulsen, J., Reyes, R., Rife, C. L., Sefcovic, N., Tien, H. J., Trame, C. B., van den Bedem, H., Weekes, D., Xu, Q., Hodgson, K. O., Wooley, J., Elsliger, M.-A., Deacon, A. M., Godzik, A., Lesley, S. A., Tainer, J. A., and Wilson, I. A. (2010) Crystal structure of the first eubacterial Mre11 nuclease reveals novel features

that may discriminate substrates during DNA repair. *J. Mol. Biol. 397*, 647–663.

(26) Williams, R. S., Moncalian, G., Williams, J. S., Yamada, Y., Limbo, O., Shin, D. S., Groocock, L. M., Cahill, D., Hitomi, C., Guenther, G., Moiani, D., Carney, J. P., Russell, P., and Tainer, J. A. (2008) Mre11 dimers coordinate DNA end bridging and nuclease processing in double-strand-break repair. *Cell 135*, 97–109.

(27) Hopfner, K.-P., Karcher, A., Craig, L., Woo, T. T., Carney, J. P., and Tainer, J. A. (2001) Structural biochemistry and interaction architecture of the DNA double-strand break repair Mre11 nuclease and Rad50-ATPase. *Cell 105*, 473–485.

(28) Hopfner, K.-P., and Tainer, J. A. (2003) Rad50/SMC proteins and ABC transporters: unifying concepts from high-resolution structures. *Curr. Opin. Struct. Biol 13*, 249–255.

(29) Jones, P. M., O'Mara, M. L., and George, A. M. (2009) ABC transporters: a riddle wrapped in a mystery inside an enigma. *Trends Biochem. Sci. 34*, 520–531.

(30) Davidson, A. L., Dassa, E., Orelle, C., and Chen, J. (2008) Structure, function, and evolution of bacterial ATP-binding cassette systems. *Microbiol. Mol. Biol. Rev. 72*, 317–364.

(31) Hopfner, K. P., Karcher, A., Shin, D. S., Craig, L., Arthur, L. M., Carney, J. P., and Tainer, J. A. (2000) Structural biology of Rad50 ATPase: ATP-driven conformational control in DNA double-strand break repair and the ABC-ATPase superfamily. *Cell 101*, 789–800.

(32) Hopfner, K.-P., Craig, L., Moncalian, G., Zinkel, R. A., Usui, T., Owen, B. A. L., Karcher, A., Henderson, B., Bodmer, J.-L., McMurray, C. T., Carney, J. P., Petrini, J. H. J., and Tainer, J. A. (2002) The Rad50 zinc-hook is a structure joining Mre11 complexes in DNA recombination and repair. *Nature 418*, 562–566.

(33) Hirano, M., Anderson, D. E., Erickson, H. P., and Hirano, T. (2001) Bimodal activation of SMC ATPase by intra- and inter-molecular interactions. *EMBO J. 20*, 3238–3250.

(34) Williams, G. J., Williams, R. S., Williams, J. S., Moncalian, G., Arvai, A. S., Limbo, O., Guenther, G., Sildas, S., Hammel, M., Russell, P., and Tainer, J. A. (2011) ABC ATPase signature helices in Rad50 link nucleotide state to Mre11 interface for DNA repair. *Nat. Struct. Mol. Biol 18*, 423–431.

(35) Gilbert, S. P., and Mackey, A. T. (2000) Kinetics: a tool to study molecular motors. *Methods 22*, 337–354.

(36) Liu, F., Dong, Q., Myers, A. M., and Fromm, H. J. (1991) Expression of human brain hexokinase in Escherichia coli: purification and characterization of the expressed enzyme. *Biochem. Biophys. Res. Commun. 177*, 305–311.

(37) Kuzmic, P. (1996) Program DYNAFIT for the analysis of enzyme kinetic data: application to HIV proteinase. *Anal. Biochem. 237*, 260–273.

(38) Bloom, L. B., Otto, M. R., Eritja, R., Reha-Krantz, L. J., Goodman, M. F., and Beechem, J. M. (1994) Pre-steady-state kinetic analysis of sequence-dependent nucleotide excision by the 3′-exonuclease activity of bacteriophage T4 DNA polymerase. *Biochemistry 33*, 7576–7586.

(39) Vistica, J., Dam, J., Balbo, A., Yikilmaz, E., Mariuzza, R. A., Rouault, T. A., and Schuck, P. (2004) Sedimentation equilibrium analysis of protein interactions with global implicit mass conservation constraints and systematic noise decomposition. *Anal. Biochem. 326*, 234–256.

(40) Rudolph, F. B., Fromm, H. J., and Purich, D. L. (1996) in *Contemporary Enzyme Kinetics and Mechanism*; Purich, D. L., Ed.

(41) Gould, A. D., Telmer, P. G., and Shilton, B. H. (2009) Stimulation of the maltose transporter ATPase by unliganded maltose binding protein. *Biochemistry 48*, 8051–8061.

(42) Tombline, G., Bartholomew, L., Gimi, K., Tyndall, G. A., and Senior, A. E. (2004) Synergy between conserved ABC signature Ser residues in P-glycoprotein catalysis. *J. Biol. Chem. 279*, 5363–5373.

(43) Hirano, M., and Hirano, T. (1998) ATP-dependent aggregation of single-stranded DNA by a bacterial SMC homodimer. *EMBO J. 17*, 7139–7148.

(44) Moncalian, G., Lengsfeld, B., Bhaskara, V., Hopfner, K.-P., Karcher, A., Alden, E., Tainer, J. A., and Paull, T. T. (2004) The rad50 signature motif: essential to ATP binding and biological function. *J. Mol. Biol. 335*, 937–951.

(45) Bhaskara, V., Dupré, A., Lengsfeld, B., Hopkins, B. B., Chan, A., Lee, J.-H., Zhang, X., Gautier, J., Zakian, V., and Paull, T. T. (2007) Rad50 adenylate kinase activity regulates DNA tethering by Mre11/Rad50 complexes. *Mol. Cell 25*, 647–661.

(46) Bareil, C., Thèze, C., Béroud, C., Hamroun, D., Guittard, C., René, C., Paulet, D., Georges, M. des, and Claustres, M. (2010) UMD-CFTR: a database dedicated to CF and CFTR-related disorders. *Hum. Mutat. 31*, 1011–1019.

(47) Chen, C.-A., and Cowan, J. A. (2003) Characterization of the soluble domain of the ABC7 type transporter Atm1. *J. Biol. Chem. 278*, 52681–52688.

(48) Fetsch, E. E., and Davidson, A. L. (2002) Vanadate-catalyzed photocleavage of the signature motif of an ATP-binding cassette (ABC) transporter. *Proc. Natl. Acad. Sci. U.S.A 99*, 9685–9690.

(49) Janas, E., Hofacker, M., Chen, M., Gompf, S., van der Does, C., and Tampé, R. (2003) The ATP hydrolysis cycle of the nucleotide-binding domain of the mitochondrial ATP-binding cassette transporter Mdl1p. *J. Biol. Chem. 278*, 26862–26869.

(50) Moody, J. E., Millen, L., Binns, D., Hunt, J. F., and Thomas, P. J. (2002) Cooperative, ATP-dependent association of the nucleotide binding cassettes during the catalytic cycle of ATP-binding cassette transporters. *J. Biol. Chem. 277*, 21111–21114.

(51) Lee, J.-H., and Paull, T. T. (2006) Purification and biochemical characterization of ataxia-telangiectasia mutated and Mre11/Rad50/Nbs1. *Methods Enzymol. 408*, 529–539.

(52) Arnold, K., Bordoli, L., Kopp, J., and Schwede, T. (2006) The SWISS-MODEL workspace: a web-based environment for protein structure homology modelling. *Bioinformatics 22*, 195–201.

(53) Koroleva, O., Makharashvili, N., Courcelle, C. T., Courcelle, J., and Korolev, S. (2007) Structural conservation of RecF and Rad50: implications for DNA recognition and RecF function. *EMBO J. 26*, 867–877.

(54) Lammens, A., Schele, A., and Hopfner, K.-P. (2004) Structural biochemistry of ATP-driven dimerization and DNA-stimulated activation of SMC ATPases. *Curr. Biol. 14*, 1778–1782.